Forsch Ingenieurwes (2023) 87:655–671
https://doi.org/10.1007/s10010-023-00610-9

ORIGINALARBEITEN/ORIGINALS

Characterisation of the conveying effect of turned radial shaft seal counter-surfaces using a simplified hydrodynamic simulation model

Stefan Thielen[1] · Thirumanikandan Subramanian[1] · Bernd Sauer[1] · Oliver Koch[1] · Richard Börner[2] · Thomas Junge[2] · Andreas Schubert[2]

Received: 23 April 2022 / Accepted: 23 December 2022 / Published online: 31 January 2023

Abstract

A typical sealing system for rotating shafts consists of the radial shaft sealing ring (RSS), the lubricant and the shaft counter-surface (SCS) of the rotating shaft. The properties of the machined surface of the SCS have an impact on the sealing system. The structural pattern of the SCS influences the lubricant flow along the axial direction. In this paper, a simplified micro scale hydrodynamic simulation model is presented in order to study and determine the axial flow of the lubricant induced by the SCS of the sealing system, isolated from the effects induced by the seal, to allow for a rating of the shaft surface. The influence of the seal was neglected to allow for a simplified simulation. Simulated shaft surfaces corresponding to different machining parameters of machined SCS are used as input. These variants of SCS were created using a kinematic model which simulates an ideal surface machining process of the shaft. A micro scale hydrodynamic simulation model is used to investigate the influence of machining parameters on the lubricant flow along the axial direction across the tribo-contact. From this investigation, the connection between parameters applied for machining of the SCS and conveying effects can be estimated. The simulation model is also validated with experimental results of hard turned shafts of different machining parameters. Differences between manufactured real surfaces and kinematically simulated surfaces are the cause of deviations between the results.

Thirumanikandan Subramanian contributed equally to this work.

✉ Stefan Thielen
stefan.thielen@mv.uni-kl.de

Thirumanikandan Subramanian
subramnian@mv.uni-kl.de

Bernd Sauer
Sauer@mv.uni-kl.de

Oliver Koch
koch@mv.uni-kl.de

Richard Börner
richard.boerner@mb.tu-chemnitz.de

Thomas Junge
thomas.junge@mb.tu-chemnitz.de

Andreas Schubert
andreas.schubert@mb.tu-chemnitz.de

[1] Chair for Machine Elements, Gears and Tribology (MEGT), Technische Universität Kaiserslautern, Gottlieb-Daimler-Str. 42, 67663 Kaiserslautern, Germany

[2] Professorship Micromanufacturing Technology, Technische Universität Chemnitz, Reichenhainer Straße 70, 09107 Chemnitz, Germany

Bestimmung des Fördereffekts gedrehter Wellenlaufflächen für Radialwellendichtringe mit einem einfachen hydrodynamischen Modell

Zusammenfassung

Ein typisches Dichtungssystem für Wellen besteht aus dem Radialwellendichtring (RWDR), dem Schmierstoff und der Dichtringgegenlauffläche (DRGF). Die Eigenschaften der gedrehten Oberfläche der DRGF haben Auswirkungen auf das Dichtungssystem. Die Oberfläche der DRGF beeinflusst den Schmierstoffffluss in axialer Richtung. In diesem Artikel wird ein vereinfachtes hydrodynamisches Simulationsmodell auf der Mikroskala vorgestellt, um die axiale Strömung des Schmierstoffs zu untersuchen und zu bestimmen, die durch die DRGF des Dichtungssystems verursacht wird, isoliert von den durch die Dichtung induzierten Effekten, um eine Bewertung der Wellenoberfläche zu ermöglichen. Die Dichtung wurde vernachlässigt um eine möglichst einfache Modellierung zu ermöglichen. Simulierte Wellenoberflächen, die verschiedenen Bearbeitungsparametern von gedrehten DRGF entsprechen, werden als Input verwendet. Diese Varianten von DRGF wurden mit Hilfe eines kinematischen Modells erstellt, das einen idealen Oberflächenbearbeitungsprozess der Welle simuliert. Ein hydrodynamisches Simulationsmodell auf der Mikroskala wird verwendet, um den Einfluss der Schnittparameter auf den Schmierstoffffluss entlang der axialen Richtung über den Tribo-Kontakt zu untersuchen. Anhand dieser Untersuchung kann der Zusammenhang zwischen den Parametern für das Drehen der DRGF und dem Fördereffekt der DRGF bestimmt werden. Das Simulationsmodell wird auch mit experimentellen Ergebnissen von hartgedrehten Wellen mit unterschiedlichen Schnittparametern validiert.

1 Introduction

Radial shaft seals are used for sealing the exit of rotating shafts of lubricated systems [39]. Their main task is to prevent the lubricant from leaking out of the working chamber and also the penetration of fluids and/or dirt particles into the working chamber [34]. The sealing function must be durable for a long period of time, since any damage during time of operation and the resulting cost of repair is much higher than the cost of the sealing ring itself. For the system to be tight, the sum of the flow components in the direction of the oil side must exceed the sum of the flow components in the direction of the air side [20]. Roughness elevations on the sealing edge lead to a conveying effect in the case of an asymmetrical distribution of contact pressure and seal distortion [32] (cf. Fig. 1). The fluid dragged along by rotation of the shaft is deflected in the axial direction at the roughness elevations.

The surface finish of the SCS has a considerable influence on the sealing system [3, 23, 40]. (In this context, the term surface finish includes the surface topography and hardness of the near surface region.) During the time of operation, it influences the wear and surface topography of the RSS. This in turn has an impact on the conveying value of the RSS, which is the ability to transfer the lubricant along the axial direction of the sealing contact. The structural pattern of the SCS also influences the flow of the lubricant in axial direction due to conveying effects [32]. As a consequence of the shaft manufacturing kinematics during turning, the SCS exhibits twist structures. During shaft rotation, these structures contribute to a transport of the lubricant to either the oil side or the air side of the RSS similar to the conveying action of a screw pump, based on the shaft rotation direction and the direction of the lead pattern of the structure. The total conveying effect of a sealing system is the sum of the effect imposed by the shaft surface and by the seal [6].

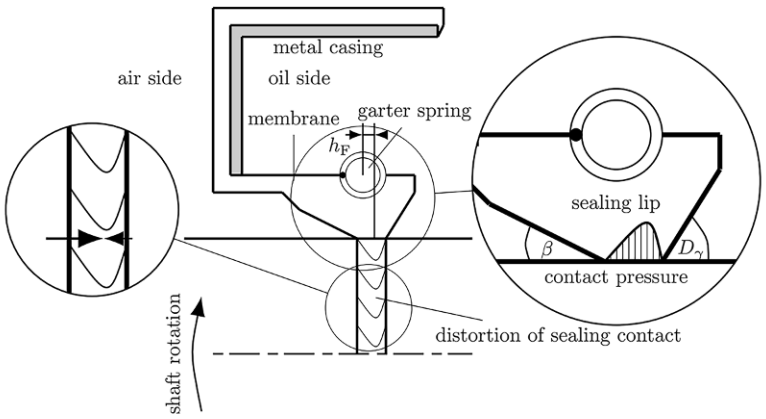

Fig. 1 Structure of the sealing system according to [39]

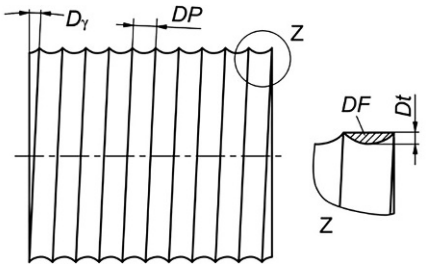

Fig. 2 Macro twist characteristics according to [28]

Generally a twist is any surface phenomenon that leads to a diversion of the fluid to be sealed [36]. A distinction is made between macro-twist and micro-twist structures [28]. Macro-twist refers to periodic, directional structures such as feed grooves. Micro-twist refers to micro-grinding structures whose main direction has a perpendicularity deviation from the shaft axis. Standardized parameters exist to describe the macro-twist [28] as shown in Fig. 2, but this is not yet the case for the micro-twist.

Stochastically occurring structures on the SCS, such as scratches caused by improper handling, are also categorized as twist, since they can lead to a conveying effect [1, 26].

A simplifying approach assuming an ideal exact circular corner radius and neglecting the minor cutting edge allows for the estimation of macro-twist parameters using geometric-kinematic relations (see Table 1) [31].

Movement of the lubricant towards either side of the RSS has impacts on the sealing system. Movement towards the oil side is considered as a tight system, since leakage is prevented. However, excessive transport of lubricant towards the oil side means starved lubrication in the region of the sealing ring contact. This leads to a local temperature rise and increased wear rate, followed by thermal damage of the RSS. Transportation of the lubricant towards the air side happens when the conveying effect is stronger than the pumping effect of RSS and leads to leakage. Thus the conveying of lubricant alongside of the RSS and SCS tribocontact needs to be balanced. In the desired state of a sealing system, the pumping is mainly done by the RSS and the SCS remains as neutral as possible.

Table 1 Relation between turning and macro-twist parameters [31]. Symbols are defined in the nomenclature

Macro-twist parameter	Relation to machining parameters
Twist angle $D_\gamma/°$	$\tan(D_\gamma) = -\frac{f}{\pi d}$
Twist depth $Dt/\mu m$	$Dt = r_\epsilon - \sqrt{r_\epsilon^2 - \frac{f^2}{4}}$
Theor. conveying cross section $DF/\mu m^2$	$DF = \frac{r_\epsilon^2}{2}(\alpha - \sin(\alpha)); \alpha = 2\arcsin\left(\frac{f}{2r_\epsilon}\right)$
Period length $DP/\mu m$	$DP = f$

Manufacturing of the SCS is usually realised by preturning, hardening and infeed grinding [8, 24]. From an economic and environmental point of view, however, grinding has numerous disadvantages such as high investment costs, low flexibility, a high proportion of non-value-added machining time due to sparking. With the development of more efficient cutting materials, grinding is increasingly replaced by machining processes with geometrically defined cutting edges, such as hard turning [12, 13, 38] or other finishing processes [40]. The main advantages of hard turning include high flexibility, the possibility of complete and dry machining and the elimination of sparking time. The basic prerequisite for successful process substitution is the guarantee of component function, which is significantly influenced by the properties of the surface. However, hard turned and ground surfaces differ considerably from one another in terms of their topography and the physical properties of the peripheral zone [2, 15, 25]. The feed helix resulting from turning, i.e. the kinematic roughness, represents a pronounced macro-twist compared to ground surfaces. This can lead to a transport of the lubricant depending on the direction of rotation. For a long time, hard-turned SCSs were therefore mostly used only in units with a fixed or dominant direction of rotation [37, 41]. Investigations of machined shaft surfaces have shown the potential to create a tight sealing system and also reduce friction and wear if the right machining parameters are chosen [10, 38]. Experimental investigations require testing of various SCS manufactured with different process parameters, which means the number of samples to be manufactured and tested are high in number. The time involved in machining and also testing the samples is therefore quite expensive. However, the identification and definition of surface parameters relevant to sealing technology, which reflect the influence of the surface finish of SCS on the functional behaviour of the sealing system with sufficient accuracy, has proven to be extremely complex [9].

This is why a simulation model is needed, where a SCS generated by a kinematic simulation can be given as input and the interaction of the topography of the surface finish with the lubricant can be simulated to determine the functional parameters of the sealing system, like conveying action. Using such a simulation, various combinations of the surface finishes of SCS can be investigated to determine and examine the influence of certain critical machining parameters and hard turning methods. With this knowledge, a reduced number of targeted experiments can be planned, with specific critical parameters and specific hard turning methods. This saves time, effort and is more cost effective than testing all combinations of relevant machining parameters of hard turning. Simulations of the lubrication of a sealing contact usually involve a full elastohydrodynamic simulation, where the hydrodynamic action of the

lubricant, but also the deformation of seal and shaft, are considered [33, 39]. For the numerical evaluation of the averaged effect a rough surface imposed on lubricant flow, PATIR and CHENG have introduced flow factors [29, 30]. They describe the ratio of the flow between smooth surfaces compared to the flow between rough surfaces for flow driven by a pressure gradient or the shearing motion due to sliding of one or both surfaces. The evaluation of flow factors usually involves hydrodynamic lubrication simulations of the smooth and rough case. HARP and SALANT have expanded the flow factor calculation by using a mass conserving cavitation model and applied it to radial shaft seals [17]. ROCKE and SALANT developed a method taking into account the angular distortion of the seal roughness due to shear forces [33]. An other option is to model the surface roughness using analytical functions. Most of such models take into account the seal topography and neglect the shaft roughness [22, 35], in order to prevent the need of a more time consuming and numerically less stable transient simulation. When the shaft topography shall be considered, usually the seal roughness is neglected [14, 19]. Only few researchers have implemented transient simulations considering the topography of both shaft and seal yet [11, 39]. Those simulation models however, have a high calculation cost and time and are not always numerically stable, especially in the mixed friction region [39]. This greatly reduces the ability to apply those detailed models for the prediction of the influence of the shaft surface on the conveying effect of the shaft from the manufacturing parameters in a setting outside of academia.

In this paper a simplified hydrodynamic model is described where the surface topography of the seal and deformation in general are neglected in order to investigate solely the influence of the SCS topography on the fluid conveyance. These simplifications allow for much easier application of the model, especially outside of the academic setting. To allow for the estimation of the conveying behaviour of SCS before manufacturing, SCS generated with a kinematic simulation model of the machining process are used as input. Since the focus is to study the influence of different surface finishes of SCS on the conveying value, we assume a smooth rigid surface as contact partner, instead of a rough deformable seal surface. Thus, the simulation model is reduced to the elements necessary to study only the influence of the SCS finish. The advantage of this approach is a significant reduction of calculation cost and time, while the disadvantage is the aforementioned neglection of the seal topography and deformation and thus the loss of predictive capabilities regarding friction and the overall pumping rate of the whole sealing system. In cases where the behaviour of the whole sealing system, including effects from the seal, is to be investigated in detail, those simplifications should not be used.

In order to verify and validate the simulation model, experiments with samples of the same surface finishes of the SCS that were simulated, are carried out.

2 Hydrodynamic simulation

2.1 reynolds and fischer-burmeister system of equations

In the sealing contact, a lubrication gap is created between shaft and seal lip in relative movement. This lubricating gap arises elastohydrodynamically [34]. In hydrodynamic lubrication, the pressure is only generated by the relative movement of the two surfaces and the associated dragging of the lubricant into this gap [39]. In fluid mechanics, REYNOLDS equation, which is derived from the NAVIER-STOKES equations, can be used to describe fluid flow mathematically for narrow gaps [16]. Cavitation is defined as the formation of a local vapor phase when the pressure in the fluid falls below a certain limit pressure. The vapor phase can consist both of vaporized lubricant and solved gases present in the lubricant, which pass into the gas phase at a certain pressure. It can have a significant influence on the lubricant flow and should therefore not be neglected when considering the lubrication gap flow. Therefore, in the simulation model, the REYNOLDS equation using a mass conserving cavitation model according to WOLOSZYNSKI [42] with the cavitation degree $\Theta = 1 - \rho/\rho_{liq}$, which describes the ratio of gas in the cavitation region, is used [42]. Here, ρ is the lubricant density, h is the lubricating gap, η is the dynamic viscosity and Θ is the cavitation degree:

$$\frac{\partial}{\partial x}\left(\frac{\rho h^3}{12\eta}\frac{\partial p}{\partial x}\right)+\frac{\partial}{\partial y}\left(\frac{\rho h^3}{12\eta}\frac{\partial p}{\partial y}\right)= \frac{(u_1+u_2)}{2}\frac{\partial\left(1-\Theta\right)\rho h}{\partial x}+\frac{(v_1+v_2)}{2}\frac{\partial\left(1-\Theta\right)\rho h}{\partial y} \tag{1}$$

Here, the velocities u_1 and u_2 represent the velocities of the surfaces in x direction. The velocities v_1 and v_2 represent the velocities in the y direction. In most cases, it is assumed that the x direction is circumferential direction and y direction is axial direction. In the hydrodynamic simulation presented here, velocity v_1 is not zero due to a slightly different choice of the coordinate system. Further explanation can be found in Sect. 4.

When applying the REYNOLDS equation to our problem, for numerical accuracy, dimensionless terms are needed, which are obtained using the relations below:

$$u_m = \frac{u_1 + u_2}{2} \qquad v_m = \frac{v_1 + v_2}{2} \qquad V_m = \frac{v_m}{u_m} X = \frac{x}{l_x}$$
$$Y = \frac{y}{l_y} \qquad H = \frac{h}{\sigma} \qquad \overline{\rho} = \frac{\rho}{\rho_0} \qquad \overline{\eta} = \frac{\eta}{\eta_0} \qquad dY = \frac{dy}{l_y}$$
$$dX = \frac{dx}{l_x} \qquad \kappa = \frac{l_x}{l_y} \qquad P = \frac{p\sigma^2}{12u_1 l_x \eta_0}$$

Here u_m is the mean flow velocity in x direction, v_m is the mean flow velocity in y direction, V_m is the dimensionless mean flow velocity in y direction, l_x is the length of the simulation area in x direction, l_y is the length of the simulation area in y direction, dx is the length of the edge of the control volume in x direction, dy is the length of the edge of the control volume in y direction, x and y are the coordinates in x and y direction respectively, X and Y are the dimensionless coordinates in x and y direction respectively, H is the dimensionless lubricating gap, P is the dimensionless pressure, Θ is the cavitation degree, $\overline{\rho}$ and $\overline{\eta}$ are the dimensionless density and dimensionless dynamic viscosity respectively, ρ_0 and η_0 are the reference density and dynamic viscosity respectively and κ is the ratio of the length of the simulation area in x and y direction.

Thus, the dimensionless formulation of (1) is:

$$\frac{\partial}{\partial X}\left(\frac{\overline{\rho}H^3}{\overline{\eta}}\frac{\partial P}{\partial X}\right) + \kappa^2 \frac{\partial}{\partial Y}\left(\frac{\overline{\rho}H^3}{\overline{\eta}}\frac{\partial P}{\partial Y}\right) = \frac{\partial\,(1-\Theta)\,\overline{\rho}H}{\partial X} + \kappa V_m \frac{\partial\,(1-\Theta)\,\overline{\rho}H}{\partial Y} \tag{2}$$

The system of equations can be solved after discretization applying the finite volume method (FVM).

$$a_e P_E + a_w P_W + a_n P_N + a_s P_S - (a_e + a_w + a_n + a_s) P_O = a_{rhs} + b_0\Theta_O - b_{wx}\Theta_w - b_{sy}\Theta_s - b_0 + b_{wx} + b_{sy} \tag{3}$$

The convective term in (3), describes a flux where the value of a point depends much more on the upstream than on the downstream points. Therefore, in order to describe the convective terms, the individual values at the edges are not linearly interpolated by the neighbouring central points, instead an upwind method [27] is usually used, which depends on the direction of flow. here, the first order upwind method shall be used.

In order to determine the cavitation degree Θ, a FISCHER-BURMEISTER equation as represented in (4) is used in addition to the REYNOLDS equation. Here, p is contact pressure and p_{cav} is the cavitation pressure:

$$p - p_{cav} + \Theta - \sqrt{(p - p_{cav})^2 + \Theta^2} = 0 \tag{4}$$

Above the cavitation pressure $p - p_{cav} > 0$, the cavitation degree is always zero ($\Theta = 0$) and in the cavitation zone, when $p - p_{cav} \leq 0$, the cavitation degree Θ varies between 0 and 1: $0 < \Theta \leq 1$ [42].

2.2 Solver

The discretized form can be used as the system of equations which needs to be solved to determine the pressure distribution and cavitation degree. For non linear systems, NEWTONS method is applied to determine the solution using the residue of the system [27]. Basically, in this method, by using local linearisation, the zero point of a function is determined by converting the function to residual form ($f(x) - b = 0$). This can be written as ($Ap - b = 0$) for the solver represented here. The RHS obtained represents the residue. Solving the system of equations (5) for both pressure distribution and cavitation degree can be performed with the JACOBI matrices of both equations.

$$\begin{pmatrix} J_{RE,P} & J_{RE,\Theta} \\ J_{FB,P} & J_{FB,\Theta} \end{pmatrix} \begin{pmatrix} \delta P^{(i)} \\ \delta\Theta^{(i)} \end{pmatrix} = \begin{pmatrix} RE \\ FB \end{pmatrix} \tag{5}$$

where (assuming $p_{cav} = 0$),

$$J_{FB,P} = 1 - \frac{P_i}{\sqrt{{P_i}^2 + {\Theta_i}^2}} \tag{6}$$

$$J_{FB,\Theta} = 1 - \frac{\Theta_i}{\sqrt{{P_i}^2 + {\Theta_i}^2}} \tag{7}$$

RE	REYNOLDS equation in residual form
FB	FISCHER-BURMEISTER equation
$J_{RE,P}$	Derivation of the REYNOLDS equation (RE) in terms of P
$J_{FB,P}$	Derivation of the FISCHER-BURMEISTER equation (FB) in terms of P
$\delta P^{(i)}$	Correction value for P in the i-th iteration step
$\delta \Theta^{(i)}$	Correction value for Θin the i-th iteration step

On solving (5), using the GAUSS-SEIDEL method, correction values of both pressure and cavitation degree can be determined. With these correction values, the dimensionless pressure distribution and dimensionless cavitation degree along the control volume can be calculated using (8) and (9) for the current iteration step i.

$$P^{(i)} = P^{(i-1)} + \omega\left(\delta P^{(i)}\right) \tag{8}$$

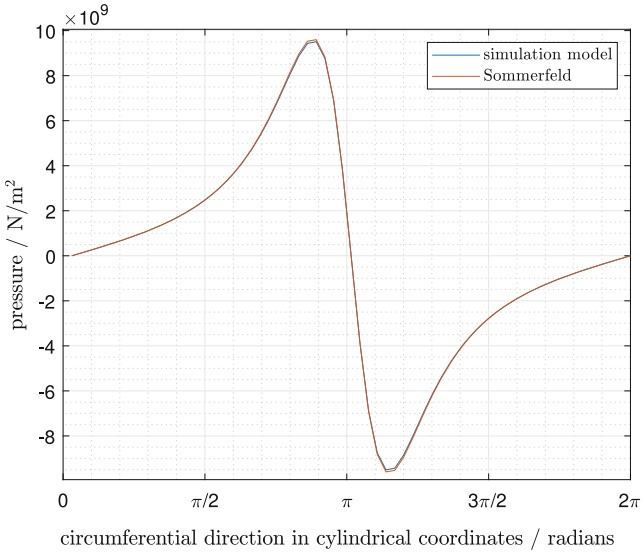

Fig. 3 Verification of the simulation model using SOMMERFELD solution

$$\Theta^{(i)} = \Theta^{(i-1)} + \omega \left(\delta\Theta^{(i)} \right) \tag{9}$$

This is repeated in iterative manner until convergence is reached. In addition to the discretization error, which depends on the grid resolution, the precision of the estimation is based on how small the convergence limit is.

Due to the neglection of the seal, in this case the application of a force balance to solve for the lubricant height is not feasible. Instead, a typical value for a lubrication film in sealing systems is used. This is a further simplification of the simulation model, which is necessary in this special case.

Before proceeding with the application of the simulation model to shaft surfaces, a validation against the analytic SOMMERFELD (cavitationless) solution of an infinitely wide journal bearing surface (10) [16] was carried out.

$$p - p_0 = \frac{6\eta_0\omega_b\left(\frac{r_b}{c}\right)^2 e \sin\phi(2 + e\cos\phi)}{(2+e^2)(1+e\cos\phi)^2} \tag{10}$$

where,

p_0	pressure at the maximum film thickness = 0 N/m²
ω_b	angular velocity of surface = 104.72 rad/s
r_b	radius of journal bearing = 40 mm
c	radial clearance of journal bearing (gap) = 15 µm
e	eccentricity ratio (distance between symmetry axis of shaft and journal bearing) = 0.75
ϕ	angle in cylindrical coordinates (circumferential)
η_0	lubricant dynamic viscosity = 14.27 mPas
l	length of journal (infinitely wide), assumed as 1×10^5 m

Since there exists no analytic solution considering mass conserving cavitation, the cavitation was deactivated in the simulation model for this purpose. Therefore, the comparison does not include a validation of the mass conserving cavitation aspect of our model. Fig. 3 shows the comparison of the analytical and numerical solution. An agreement of 99.65%, or an error of 0.35%, respectively was achieved for the cavitationless solution.

3 Kinematic simulation and manufacturing of shaft surfaces

The SCS kinematic simulation serves as input for the hydrodynamic simulation. It is built on a dexel based model which was first introduced and described for the simulation of milling operations in [4, 5]. Since physical effects such as burr formation, chipping as well as cutting forces or temperatures are not considered it is called 'kinematic simulation'. The tool, which is represented in simplified form by its cutting edge contour, is moved through the workpiece volume according to its movement trajectory. Any intersecting volume is subtracted from the workpiece volume leaving a track of the cutting edge. The simulation is implemented by modelling both workpiece and tool in a dexel-based data model. For the current investigations the simulation principle was adjusted for turning operations. Using this model, the surfaces were simulated according to Table 2.

Variations include different values for feed, corner radius, shaft diameter and as the comparison of conventional cutting tools vs. cutting tools with special wiper geometry, which is used to produce a reduced surface roughness compared to conventional tools [7]. Variants 9 and 10 use the same machining parameters as variant 3 and 4, the only difference is the use of a wiper geometry instead of a tool with a conventional corner radius (Fig. 4). This results in signif-

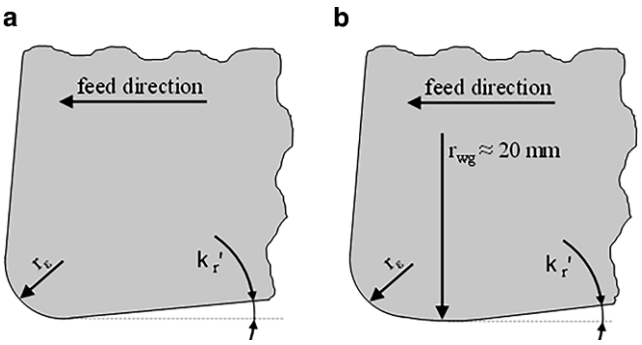

Fig. 4 Comparison between **a** conventional corner radius **b** and cutting geometry with wiper as a significantly larger radius transition to the minor cutting edge (tool reference plane)

Table 2 Machining parameters and surface characteristics

Variant	Shaft Dia (mm)	Feed (µm)	Corner radius (µm)	DF (µm^2)	Rq$_{avg}$ (µm)	Rz$_{avg}$ (µm)	Twist depth (µm)	Twist angle (°)
1	80	55	400	34.2	0.32	1.39	1,08	0.013
2	80	115	400	193	0.89	3.20	2.75	0.026
3	80	80	800	55.7	0.34	1.64	1.16	0.018
3.1*	40	80	800	39.88	0.29	1.32	0.79	0.015
3.2*	100	80	800	42.13	0.30	1.46	0.80	0.036
4	80	160	800	316	1.06	3.81	3.3	0.036
5	80	100	1200	70.6	0.35	1.45	1.05	0.023
6	80	200	1200	471	1.25	4.57	3.75	0.046
9**	80	80	800	6.5	0.09	0.55	0.18	0.018
10**	80	160	800	23.4	0.13	0.79	0.34	0.036

* Variants with same machining parameters as variant 3 but with different shaft diameters,
** Wiper geometry variants

icantly reduced values of roughness Rz and is expected to also influence the conveying action.

As long as the shaft diameter remains constant, the twist angle only depends on the feed (see Table 1). Therefore, variants 3.1 and 3.2 with 40 mm and 100 mm shaft diameters and consequently different twist angle as variant 3 have been investigated as well.

The variants listed in Table 2 were also manufactured in order to perform reverse pumping experiments. The amount of possible experiments was limited and did not permit investigation of further parameter sets. The alloyed case hardening steel 16MnCr5 was used for the investigations. The specimens were in case-hardened state (hardness 56 HRC, case hardness depth 0.8 mm). After pre-machining, the specimens were characterised by a diameter of 80.1 mm. For the machining experiments, cubic boron nitride (CBN) tipped indexable inserts of the type CCGW09T3 were used. The cutting material of the inserts contains approx. 65%–70% of CBN particles with an average grain size of 4 µm and TiN as binder. Furthermore, the inserts are coated with a TiAlN/TiCN layer offering a thickness of 2 µm. Standardized indexable inserts with a clearance angle of $\alpha = 7°$, a rake angle of $\gamma = 0°$ and a tool included angle of $\epsilon_r = 80°$ were used. The cutting edge contains a negative chamfer with a width of 0.12 mm and a chamfer angle of 25°. In combination with the tool holder used a tool cutting edge angle of the minor cutting edge of $\kappa m_r' = 5°$ results. In addition to the feed rate, the corner radius (r_ϵ) was varied in three equal steps in the range from 400 µm to 1200 µm in order to investigate the influence of different kinematical surface roughness on the hydrodynamic properties. Furthermore, standardised indexable inserts with a wiper geometry were used. They contain an arc-shaped transition from the corner radius to the minor cutting edge that is visualized in Fig. 4 in comparison to a standard geometry without modified minor cutting edge. The radius of this arc is significantly larger than the corner radius and determines the theoretical roughness. Thus, a significantly smaller surface roughness can be achieved with the same cutting parameters. An additional advantage of this wiper geometry form is that it is less sensitive to deviations from the theoretical cutting edge angle of the minor cutting edge. The machining experiments were conducted on a precision lathe of the type SPINNER PD 32. In the finish machining experiments the feed was varied as shown in Table 2. Lower feeds should lead to a decrease of the kinematical surface roughness and thus to a smaller reverse pumping value. The cutting speed and the depth of cut were kept constant at 180 m/min and 0.05 mm, respectively, since they do not change the outcome of the kinematic simulation. This last turning step was performed without any lubrication as it is usual for hard machining of steels. The geometrical properties of the machined surfaces were measured using a stylus instrument type Mahr LD 120. The stylus was characterized by a spherical radius of 2 µm and an included angle of 90°. After finish machining, the surface roughness of all specimens was measured at three positions offset by 120° in the circumferential direction with respect to the direction of the feed motion. The measuring length was 4 mm. The filtering of the profiles was done in accordance with ISO 11562 [18].

4 Flow simulation model – application and evaluation methods

The flow simulation model was built in MATLAB based on the equations discussed in Sect. 2. The structure of the model is shown in Fig. 5. The kinematic model of the SCS is used as input for the flow simulation model.

The size, the orientation and the position of the simulation area in the kinematic model influence the results

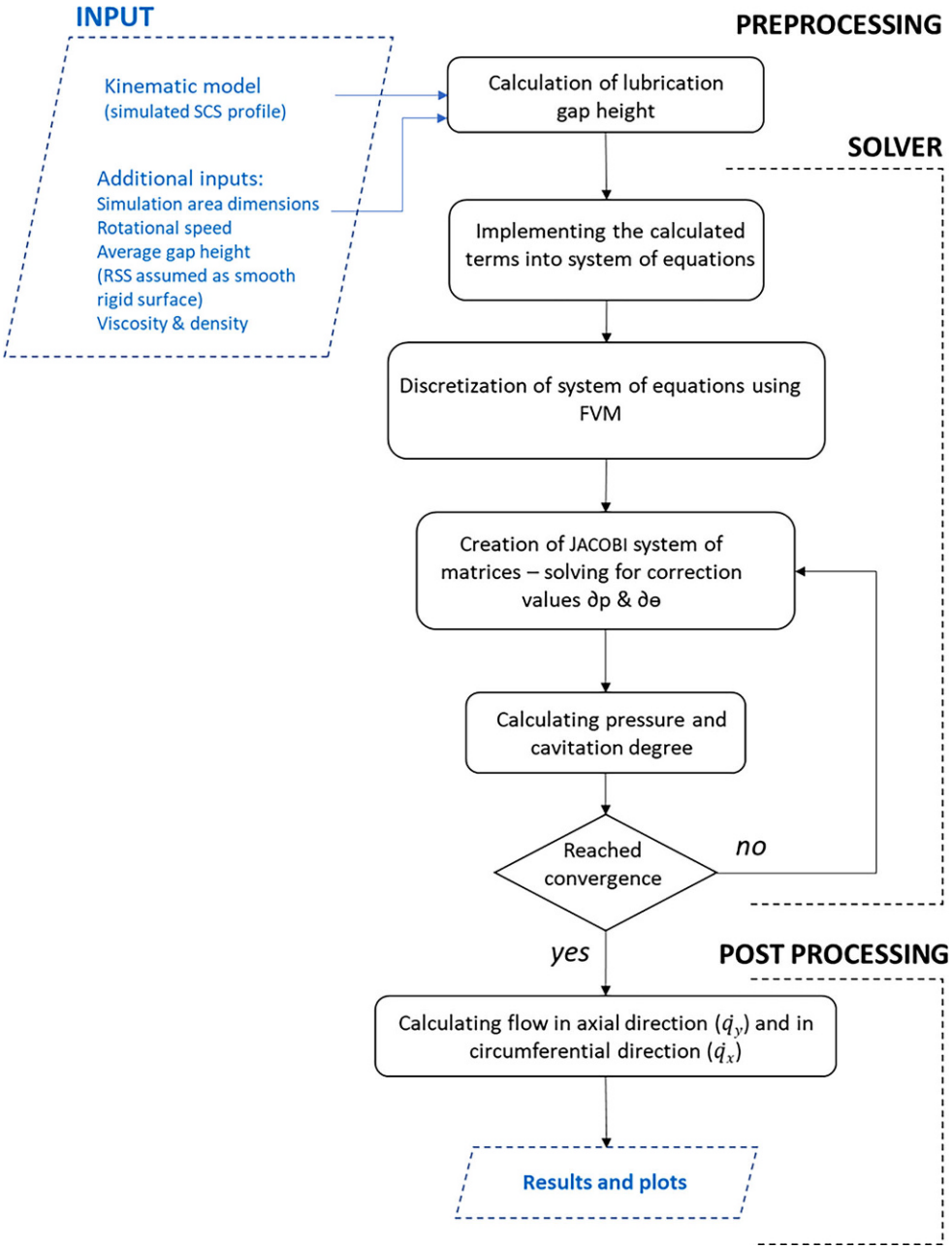

Fig. 5 Process flow of the simulation model to determine flow in axial and circumferential direction

of the hydrodynamic simulation. In order to perform the numerical calculations, the simulation domain needs to be represented by a grid with a given resolution, which is limited by the computer's computational power and memory. In our case, a regular grid with equally spaced elements is used.

Since the twist angle is extremely small, the cross section of the turning structure can not be represented with good accuracy, using a reasonable resolution. This is because of the difference in the orientation between simulation area and the twist of the surface.

If the grid is oriented along the axial (y) and circumferential (x) direction, as it usually is in similar applications [39], the minimum twist angle $D_\gamma^{\min}$ that could be represented by such a grid on a simulation area can be calculated as follows :

$$D_\gamma^{\min} = \arctan\left(\frac{dy}{l_x}\right) \tag{11}$$

with dy as distance between grid points in axial (y) direction and l_x as length of the simulation domain in circumferential direction. In order to satisfyingly represent the geometrical features of the twist structure, an significantly higher resolution would be necessary, which would strongly depend on the twist angle. With the grid described

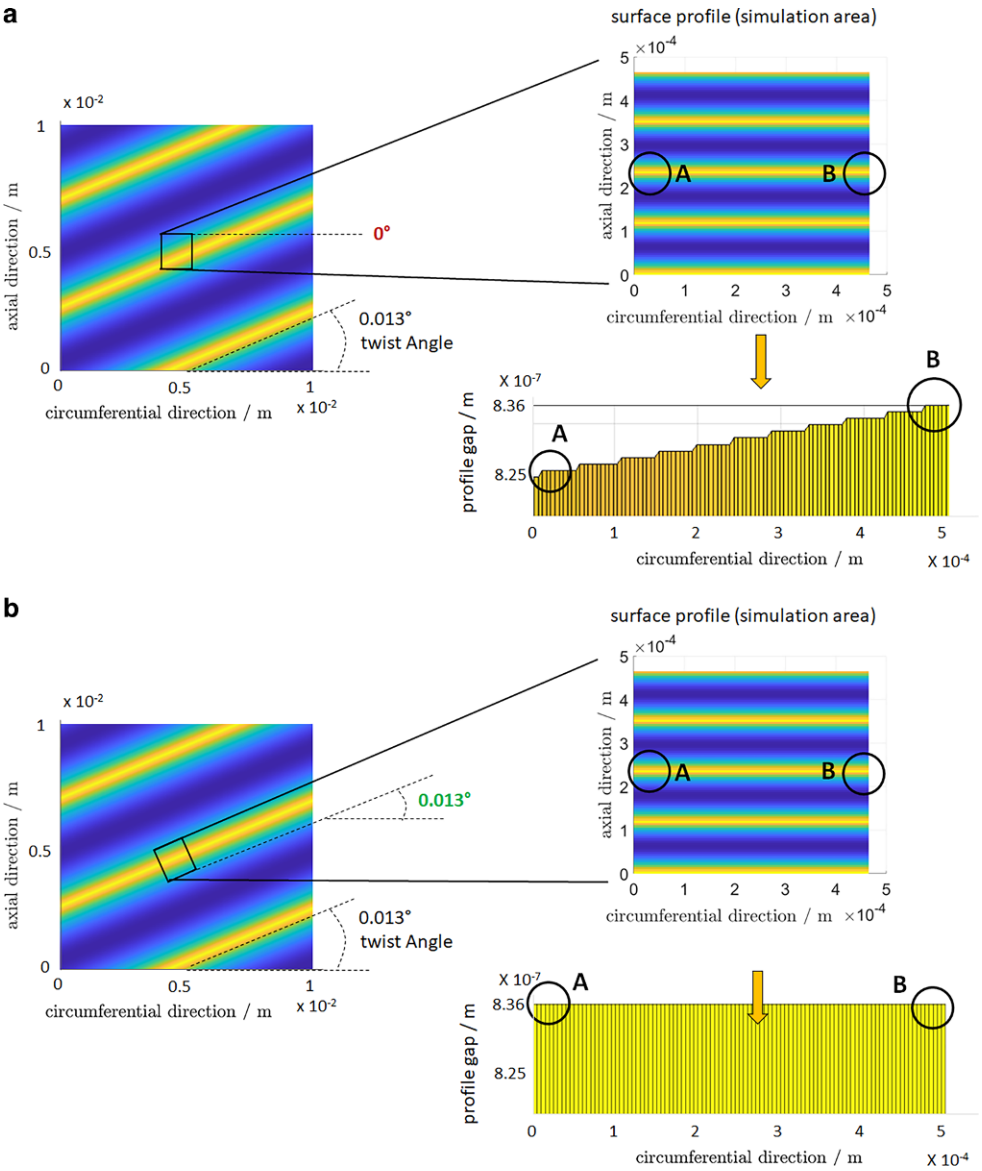

Fig. 6 Effect in the profile gap, t.: when simulation area is not in orientation with twist angle, the ridge of the structure forms an artificially step-like shape. b.: when simulation area is oriented along the twist angle, this problem does not occur

in Sect. 6.1 follows $D_\gamma^{\min} = 0.0099$, which is not $\ll D_\gamma$ of the investigated shafts (see Table 2).

In such a simulation domain and grid, this resolution dependence leads to a poor representation of the shaft surface geometry as can be seen by the step-like variation in height of the profile across the circumferential direction in Fig. 6.

To eliminate this problem the grid is oriented along the twist direction as shown in Fig. 6b. Thereby, the dependence of the grid resolution on the twist angle and also the poor representation of the shaft surface can be eliminated.

Based on this approach, the surface data for the planned SCS variants were simulated. The rotation of the simulation domain by angle D_γ also requires that the surface velocities in relation to the simulation grid u and v are recalculated (with u' and v': axial and circumferential direction in local coordinate system of the shaft, see also Fig. 13):

$$u = u' \cos(D_\gamma) + v' \sin(D_\gamma) \tag{12}$$

$$v = v' \cos(D_\gamma) + u' \sin(D_\gamma) \tag{13}$$

The same must be taken into account, when analysing the flow velocities in the lubrication gap, which can be calculated from the simulation results.

4.1 Evaluation of functional behaviour in sealing system

In order to derive the functional behaviour of a shaft surface in a sealing system, simulations are performed with different shaft rotation speeds and gap heights within the typical range for radial shaft seals [34, 39]. The simulation yields

the distribution of cavitation degree and pressure, which then needs to be further evaluated to determine conveying action and assess the lubrication properties of the surface.

4.1.1 Rate of flow and conveying action

The conveying effect that the shaft surface imposes on the lubricant can be determined by calculating the fluid flow (per volume element) in axial direction using (14) and (15) [29], where $\dot{q}_x$ and $\dot{q}_y$ are the flow rates in x- and y- direction respectively. dx and dy are the edge lengths between the discretization points.

$$\dot{q}_y = \left(\frac{-1}{12\eta}\frac{\partial p}{\partial y}h^3 dx\right) + \left((v_2 + v_1)\frac{h}{2}\Theta dx\right) \tag{14}$$

$$\dot{q}_x = \left(\frac{-1}{12\eta}\frac{\partial p}{\partial x}h^3 dy\right) + \left((u_2 + u_1)\frac{h}{2}\Theta dy\right) \tag{15}$$

After determination of total flow rate in x- and y- direction by integration along the respective diagonal direction, the resulting flow rate $\dot{q}_{ax}$ in axial and $\dot{q}_{circ}$ in circumferential direction has to be calculated using the simple trigonometric relations shown in Fig. 13 and (12), (13). The flow rate $\dot{q}_{ax}$ in axial direction was subsequently scaled to the whole shaft circumference and normalized with respect to the sliding distance (yielding a dimension of µl/m) to allow for a comparison to the reverse pumping rate results (Sect. 5.1), as shown in (16):

$$q_{ax} = \dot{q}_{ax}\left(\frac{\pi d}{l_x}\right)\left(\frac{1000\pi d}{60}\right) \tag{16}$$

where,

l_x width of the simulation surface = 5×10^{-4} m
d diameter of the shaft = 80 mm

5 Experimental setup and investigation

In order to determine the influence of the machining parameters on the conveying action of the hard turned samples and also for comparison with simulation results, reverse pumping values of shafts finish-machined with different combinations of cutting parameters were evaluated and studied to conclude on the cutting parameter dependencies. RSS of type BAUM 5X7 80-100-10 made of the fluoro-elastomer 75 FKM 585 and a PAO lubricant with SAE viscosity grade 0W-20 (η = 14.27 mPas at 70 °C) were used for all investigations.

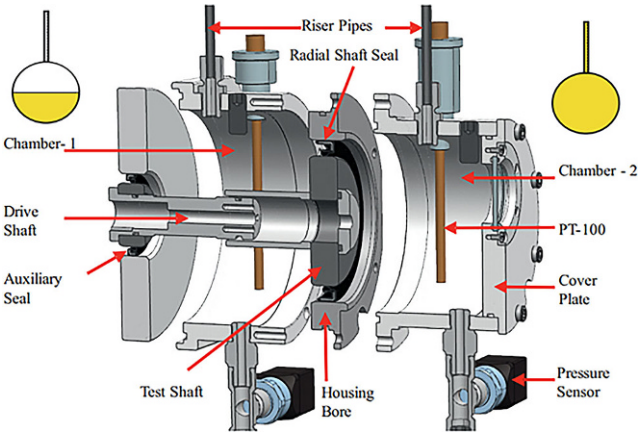

Fig. 7 Test setup for measuring the reverse pumping using the two chamber principle [6]

5.1 Reverse pumping value measurement

The test setup is made up of two test chambers as shown in Fig. 7. Every test was conducted with test chamber 2 (right) filled fully with oil and the riser pipe attached with the test lubricant, while in test chamber 1 (left), the oil was just filled up to the height of the shaft centre representing the actual application [23] In each of these chambers, the oil pressure is measured and monitored with a high resolution pressure sensor. Since the oil pressure depends on the oil level in the riser pipe, the rate of fluid transport into or out of the test chamber is determined. The method of measuring is based on the converse installation of the radial shaft seal [6, 21]. The air side of the RSS was directed towards chamber 2, resulting in a conveyance effect from chamber 2 to chamber 1. The temperatures of both oil chambers were controlled using two separate heating circuits. Before the start of the experiment, the RSS performed a 100 km run-in at 5 m/s (1189 rpm). A thermal equilibrium between both test cells is ensured before the start of the actual measurement. As a result of the reverse pumping effect, the initially filled riser pipe is emptied by the transfer of lubricant to the other chamber. This concludes the test. As the oil level in the riser pipe decreases linearly, the measured pressure also decreases. The test is run in both directions in order to determine the reverse pumping value for both SCS and RSS separately as described below. For statistical purposes, each measurement is repeated once.

The reverse pumping value of the system consisting of SCS and seal can be calculated using (17), where d_{RP} is the diameter of the riser pipe, K is the gradient of the pressure signal in oil chamber 2, ρ the density of the lubricant at test temperature, g the gravitational constant (g = 9.81 m/s^2) and v the relative speed in the sealing contact. The resulting

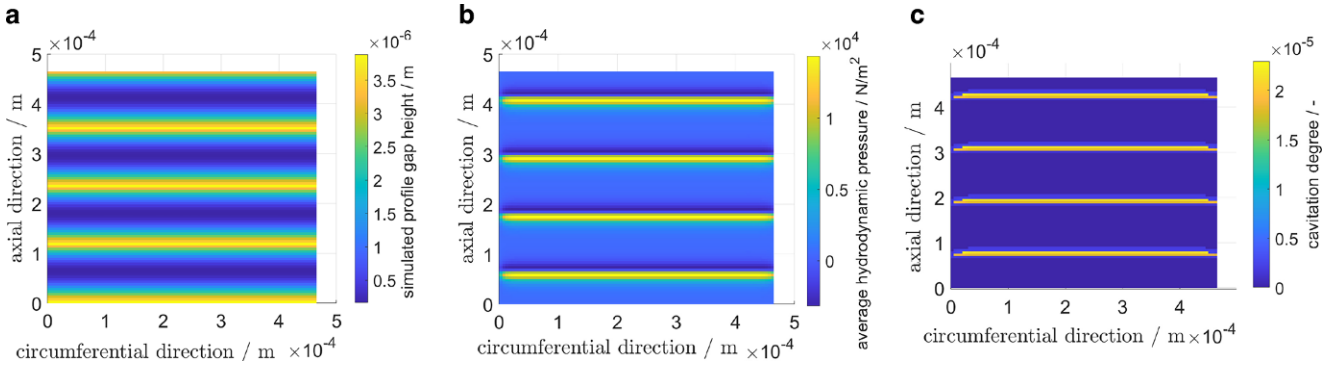

Fig. 8 Exemplary results of the simulation of variant 2 with feed f = 115 µm, twist angle D_γ = 0.026°, tool corner radius r_ϵ = 400 µm at 1000 rpm and an average gap height of 1.51 µm **a** Simulated SCS profile gap of variant 2 (after orientation along twist angle) **b** pressure distribution **c** cavitation

reverse pumping value was normalized with respect to the sliding distance and is given in µl/m [6, 40].

$$PV = \frac{\pi}{4}\frac{K d_{RP}^2}{\rho g v_r} \tag{17}$$

By using (18) and (19), the individual reverse pumping values of both SCS and RSS can be determined [40].

$$PV_{RSS} = \frac{1}{2}(PV_{Sys1} + PV_{Sys2}) \tag{18}$$

$$PV_{SCS} = \frac{1}{2}(PV_{Sys1} - PV_{Sys2}) \tag{19}$$

Here, PV_{Sys1} represents the reverse pumping value of a sealing system with SCS rotating in counter-clockwise direction and PV_{Sys2} represents the reverse pumping value of sealing system with SCS rotating in clockwise direction. PV_{RSS} is the reverse pumping value of the RSS alone, similarly, PV_{SCS} is the reverse pumping value of the SCS.

6 Results

6.1 Simulation

Hydrodynamic simulations with the SCS generated using the kinematic simulation according to Table 2 have been conducted and evaluated as described in Sects. 2 and 4. The input parameters for the simulation are listed below:

l_y	length of the simulation surface = 5×10^{-4} m
l_x	width of the simulation surface = 5×10^{-4} m
n_y	grid size along length of simulation surface = 101 cells*
n_x	grid size along width of simulation surface = 101 cells*
*	this resolution has proved to be sufficient for the investigated surfaces in a mesh convergence analysis
d	diameter of the shaft = 80 mm
u	investigated range of rotational shaft speed = 1000 rpm to 4000 rpm
h_g	investigated range of average gap heights = 0.5 µm to 2.0 µm

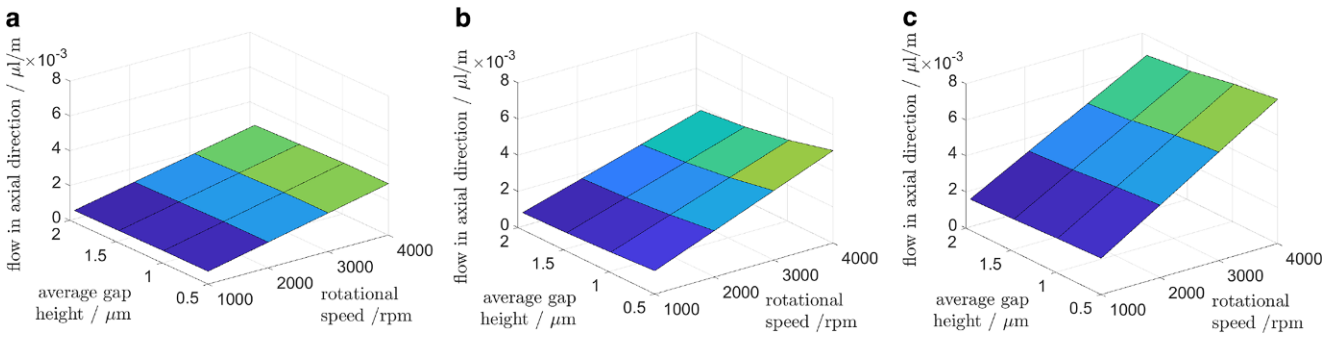

Fig. 9 Flow in axial direction of three shaft surface variants vs. average gap height and rotational speed **a** Variant 1 with feed = 55 µm, tool corner radius = 400 µm, **b** Variant 3 with feed = 80 µm, tool corner radius = 800 µm, **c** Variant 5 with feed = 100 µm, tool corner radius = 1200 µm. (see Table 2 for all surface characteristics)

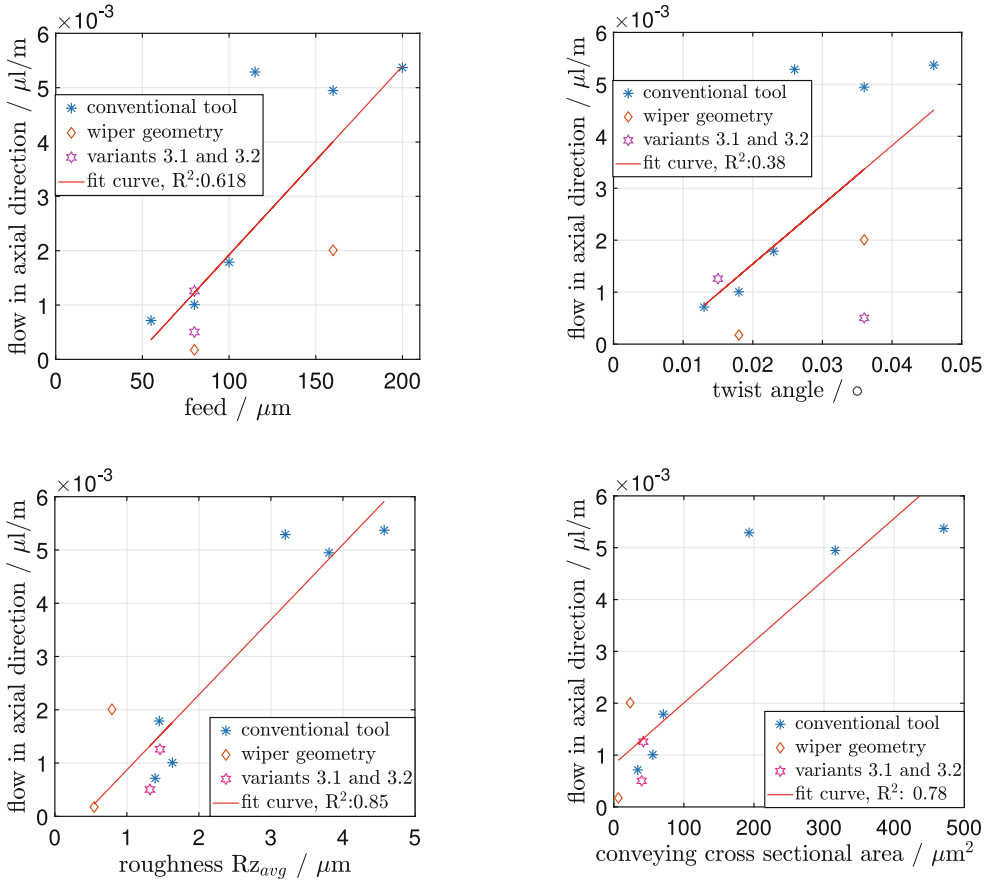

Fig. 10 Simulated fluid flow varying with different feed, twist angle, roughness and conveying cross section for rotational speed = 1000 rpm and gap height = 1.51 µm, including a linear regression and the coefficient of determination

η dynamic viscosity of lubricant = 14.27 mPas at 70 °C
ρ density of lubricant = 801.5 kg/m^3

The results are presented in this chapter and compared to experimental results obtained with manufactured SCS.

In Fig. 8a, the simulated surface of SCS of variant 2 after orientation as explained in Sect. 4 is depicted. The corresponding pressure distribution and cavitation degree distribution obtained from simulating this surface according to Sects. 2 and 4 can be seen in Fig. 8b and c. Fig. 8 serves as exemplary depiction of the primary results (pressure and cavitation) of the hydrodynamic simulation. From the pressure and cavitation distribution and the gap height, the local fluid flow can be calculated using (14), (15) and (16).

6.1.1 Numerical simulation of the fluid flow induced by the shaft surface

Fig. 9 shows the overall flow in the simulation domain in axial direction for variants 1, 3 and 5 for shaft speeds varying from 1000 rpm to 4000 rpm and average gap height varying from 0.5 µm to 2.0 µm. The average axial lubricant flow of SCS increases strongly with rotational speed and increases slightly with decreasing gap height, indicating, that the conveying effect of the SCS is stronger for smaller gap heights. Furthermore, it also increases with increasing feed (and thus higher twist angle and conveying cross section). This represents the expected behaviour.

In order to determine the influence of the machining parameters and resulting surface topography of the shaft surface, further simulations were limited to a constant speed of 1000 rpm and average gap height of 1.51 µm. The flow q_{ax} in axial direction was determined and analysed.

In Fig. 10, the flow of the lubricant in axial direction is depicted over the feed, twist angle, roughness Rz and conveying cross sectional area. Here, the roughness of the SCS manufactured with same parameters has been used, when available, since the calculation of twist depth is not valid for tools with wiper geometry, i.e. variant 9 and 10. It can be observed that the flow increases with all of those parameters. The best coefficient of determination of a linear fit R^2 can be found with roughness and conveying cross section area.

The results for variants 3.1 and 3.2 with different shaft diameters show, that the flow depends much more on the roughness Rz than on the twist angle. Furthermore, it can be seen, that SCSs which have been machined using a wiper geometry (and thus have significantly reduced values of roughness Rz, see Table 2, Var. 9, 10) have reduced ax-

Table 3 Coefficient of determination of linear regression R^2 and adjusted coefficient of determination of linear regression (considering 3 machining parameter dependencies) R^2_{adj} between simulation results and SCS parameters for all variants

Simulation result	Feed	Corner radius	Twist angle	Rz_{avg}	*DF*	Rq_{avg}
R^2 Flow q_{ax}	0.618	0.009	0.38	0.85	0.78	0.88
R^2_{adj}Flow q_{ax}	0.43	-0.49	0.065	0.77	0.67	0.82

ial flow rates compared to their corresponding conventional tool variants with same machining parameters (Var. 3 and 4). For a conventional tool geometry, the flow depends strongly on the roughness and conveying cross sectional area and depends less on feed and twist angle. However, the wiper geometry variants slightly deviate from the linear regression for both parameters. This is probably due to the fact, that the conveying action also depends on the feed (Table 1) and thus the twist angle, which is not influenced by the use of a wiper geometry.

The coefficient of determination of a linear fit between flow and corner radius of the tool was poor and is therefore not shown. However, an increase of flow with corner radius could be found when comparing SCS variants with similar feed, indicating that the corner radius has a minor effect compared to the feed.

Since the fluid flow depends on several machining parameters, the adjusted coefficient of determination taking into account dependencies with three independent parameters (d, f, r_e; all other investigated parameters are dependent on these three values in an idealized turning process) $R^2_{adj} = 1 - (1 - R^2)\frac{n-1}{n-p-1}$ (with n = number of data points, p = number of independent parameters) has also been calculated (Table 3). Results show, that especially for the twist angle R^2_{adj} is much lower and that if even becomes negative for the corner radius.

Summarizing, it can be concluded, that the flow depends on all investigated parameters with different strength and also that there exist cross dependencies between those parameters.

Dependencies between the machining parameters and hydrodynamic lift-off pressure could not be found using this simplified simulation approach. This is probably due to the choice of a fixed average gap height, since the lift-off pressure strongly depends on the gap height. Furthermore, in sealing systems, a part of the contact load is borne by direct roughness contact [39] which was also neglected.

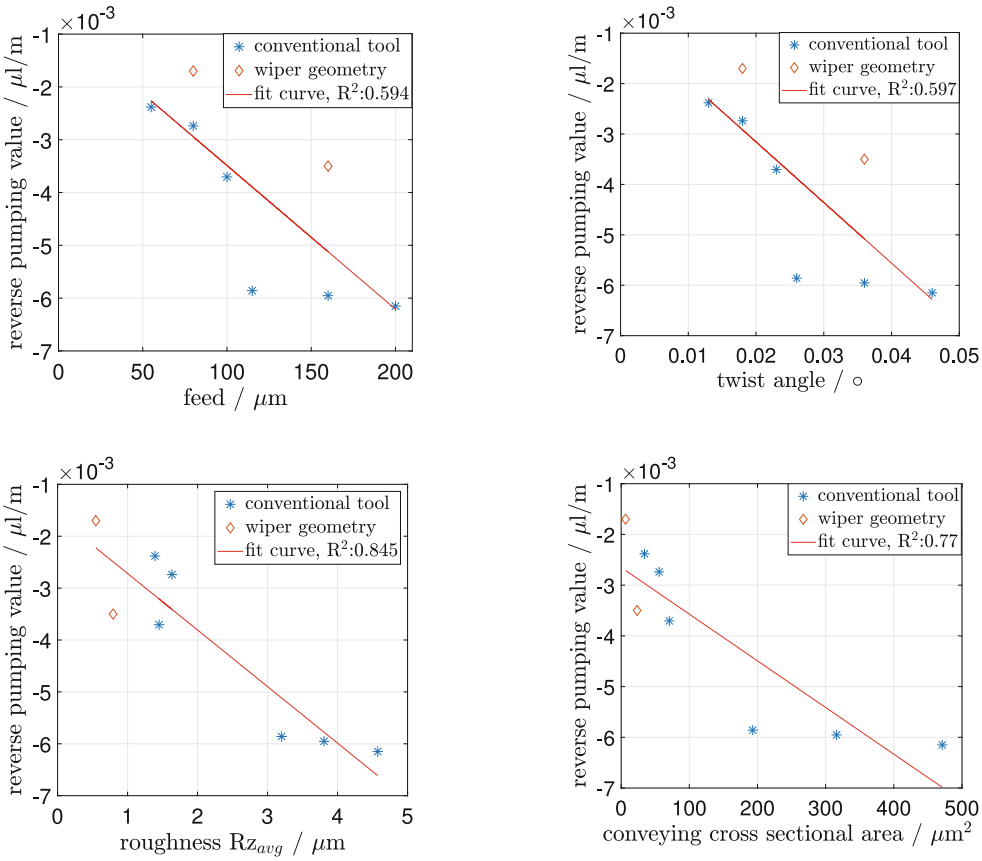

Fig. 11 Comparison of the measured reverse pumping values from experiments. Rotational speed = 1000 rpm. *t. l.*: Reverse pumping value over feed. *t. r.*: Reverse pumping value over twist angles. *b. l.*: Reverse pumping value over roughness. *b. r*: Reverse pumping value over conveying cross-sectional area

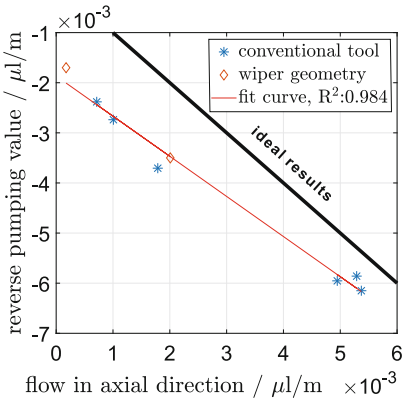

Fig. 12 Comparison of regression of measured reverse pumping value vs. simulated flow in axial direction to the ideal results. A deviation to the ideal results is present, which is significant especially for low shaft roughness

6.2 Experiment

6.2.1 Reverse pumping value

The reverse pumping values of the individual SCS, determined normalized with the sliding distance as described in Sect. 5.1, are shown in Fig. 11. The negative sign indicates fluid conveyance from air to oil side.

In agreement with the simulation of the conveying effect (Fig. 10), the measured absolute reverse pumping values, the strongest dependencies are with roughness and conveying cross sectional area. Small deviations between the behavior in simulation and measurement can be found for feed and twist angle. These deviations can be explained by the difference between the surfaces generated by the kinematic simulation (simulation input) and the manufactured surface (input for measurements). Since a kinematic simulation neglects tool vibration and plastic material behaviour during cutting, the real surface has a different roughness and cross sectional area than the simulated surface although the same feed has been used.

In order to compare simulation and experimental results, the measured reverse pumping value and simulated flow are depicted in Fig. 12. The coefficient of determination of a linear fit between both data sets of $R^2 = 0.984$ indicates that the simulation can predict the general behavior of the real manufactured surface with reasonable accuracy. However, a deviation between the absolute values is present, especially for the shafts with lower roughness. Possible reasons for these deviations are the differences between the manufactured surfaces and the kinematic simulations, which do not consider elastic and plastic deformations of the material, tool wear or vibration. A comparison of the roughness of the simulated and manufactured SCS has shown, that the deviation between both values is of the same magnitude as the deviation between the simulated fluid flow and measured pumping rates. In concordance with the relative deviation between flow simulation and measurement, for surfaces with lower roughness, the relative deviation between simulated and manufactured surface is bigger than for surfaces with higher roughness. The relative deviations match very well in their order of magnitude. This justifies the conclusion, that the deviations depicted in Fig. 12 are the result of differences between kinematic simulation and real manufactured surfaces.

The simplifications made in the hydrodynamic simulation, i.e. neglection of RSS surface, deformation and calculation of the oil viscosity based on the oil sump temperature might also result in minor prediction errors. The choice of a fixed average gap height for all surfaces in the simulation could also play a role. It is plausible, that the real gap height is smaller for surfaces with lower roughness values.

Nevertheless, the results show, that the general influence of the SCS on the fluid flow can be estimated even before shafts are machined using surfaces generated from a kinematic simulation with reasonable accuracy. This already allows for the qualitative comparison of different manufacturing parameters. Considering tool vibrations and wear in the kinematic simulation in order to get a more realistic estimation of the manufactured surface could further improve the prediction quality of the modeling approach.

7 Summary and outlook

A simplified hydrodynamic simulation model has been set up to investigate the effect of different machining parameters on the function of shaft surfaces in sealing systems using radial shaft seals. The simplifications include the neglection of seal topography, deformation, force balance and mixed friction. The fluid conveying effect in axial direction has been investigated in shaft surfaces generated with a kinematic turning simulation model.

Using the model, it could be shown that the axial flow rate, which represents the conveying effect of the surface within a sealing system, strongly depends on the shaft roughness Rz and the conveying cross sectional area *DF*

and also slightly on the twist angle D_γ and the feed f. The investigation of additional parameter sets was not possible in the scope of the work presented in this paper but could improve and expand the findings further in future work.

A comparison to measured reverse pumping values of hard turned shaft surfaces shows that the simulative predictions for the axial flow rates fit well with the behaviour in a real sealing system. Deviations between the results of flow simulation and reverse pumping value measurement were shown to be caused by differences between the roughness of simulated and manufactured shaft surfaces.

The proposed simulation model can be applied to pre-estimate the effects of the different machining parameters on the conveying action of a shaft in sealing systems and thus allow manufacturers to pre-select promising parameter sets. The model will also be used to investigate shaft surfaces generated with special turning kinematics, which are supposed to generate a lead-free surface in our upcoming research.

8 Appendix

8.1 Transfer between shaft coordinate system and twist coordinate system

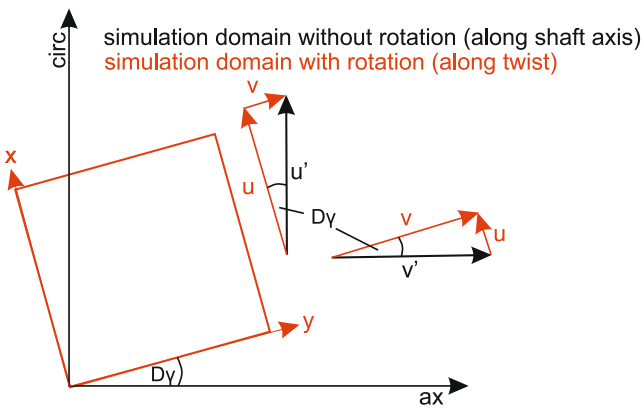

Fig. 13 Geometric relationships between the velocities in simulation domain along the shaft axis and the simulation domain along the twist direction. The angle of rotation between both systems is D_γ

8.2 Nomenclature

Table 4 Nomenclature

Symbols	Description	Unit
c	Radial clearance of journal bearing (lubricating gap)	m
d	Shaft diameter	mm
d_{RP}	Diameter of the riser pipe of the test setup to determine reverse pumping value	m
d_x	Edge length of control volume in x direction	m
d_y	Edge length of control volume in y direction	m
e	Eccentricity ratio	–
e	Discretization on eastern edge of control volume	–
ϵ_r	tool included angle of cutting insert	°
f	Feed of the turning process	mm/rev
g	Gravitational constant	m/s^2
h	Lubrication gap height	m
h_g	Range of average gap heights	µm
l	Length of journal	m
l_x	Length of simulation area	m
l_y	Width of simulation area	m
n_x	Grid size along length of simulation surface	–
n_y	Grid size along width of simulation surface	–
n	Discretization on northern edge of control volume	–
p	Contact pressure	N/m^2
p_{max}	Pressure at maximum film thickness	N/m^2
p_{cav}	Cavitation pressure	N/m^2
q_s	Cell thickness of the simulation area	m
q_{ax}	Lubricant flow in axial direction	µl/m
$\dot{q}_{ax}$	Rate of lubricant flow in axial direction	m^3/s
$\dot{q}_{circ}$	Rate of lubricant flow in circumferential direction	m^3/s
$\dot{q}_x$	Rate of lubricant flow in x direction	m^3/s
$\dot{q}_y$	Rate of lubricant flow in y direction	m^3/s
r_b	Radius of journal	m
r_e	corner radius of the cutting insert	mm
s	Discretization on southern edge of control volume	–
u'	Surface velocity in circumferential direction	m/s
u	Flow velocity in input in x direction	m/s
u_2	Flow velocity in output in x direction	m/s
u_m	Mean flow velocity in x direction	m/s
v'	Surface velocity in axial direction	m/s
v	Flow velocity in input in y direction	m/s
v_2	Flow velocity in output in y direction	m/s
v_m	Mean flow velocity in y direction	m/s
v_r	Relative speed in sealing contact	m/s
w	Discretization on western edge of control volume	–
x	Coordinate in x direction	m
y	Coordinate in y direction	m
z	Coordinate in z direction	m

Table 4 (Continued)

Symbols	Description	Unit
α	clearance angle of the tool	°
$\delta P^{(i)}$	Correction value for P in the i-th iteration step	–
$\delta \Theta^{(i)}$	Correction value for Θ in the i-th iteration step	–
η	Dynamic viscosity	Ns/m^2
η_0	Reference dynamic viscosity	Ns/m^2
$\overline{\eta}$	Dimensionless dynamic viscosity	–
κ	Ratio of the length of the simulation area in x and y direction	–
κ_r'	tool cutting edge angle of the minor cutting edge	°
ρ	Density	kg/m^3
ρ	Reference density	kg/m^3
$\overline{\rho}$	Dimensionless density	–
Θ	Cavitation degree	–
ω_b	angular velocity of bearing surface	rad/s
DF	Theoretical conveying cross-sectional area	m^2
DP	Period length	µm
Dt	Twist depth	µm
D_γ	Twist angle	°
H	Dimensionless lubrication gap height	–
$J_{RE,P}$	Derivation of the REYNOLDS equation (RE) in terms of P	–
$J_{FB,P}$	Derivation of the FISCHER-BURMEISTER equation (FB) in terms of dimensionless pressure P	–
K	the gradient of the pressure signal in oil chamber of the test setup to determine reverse pumping value	Pa/s
M	Number of cells in the width of the simulation area	–
P	Dimensionless pressure	–
PV	Reverse pumping value	µl/m
PV_{RSS}	Reverse pumping value of RSS	µl/m
PV_{SCS}	Reverse pumping value of SCS	µl/m
PV_{Sys1}	Reverse pumping value of sealing system with both SCS and RSS rotating in counterclockwise direction	µl/m
PV_{Sys2}	Reverse pumping value of sealing system with both SCS and RSS rotating in clockwise direction	µl/m
Rq_{avg}	RMS average of the SCS	µm
Rz_{avg}	Average maximum height of the SCS	µm
V_m	Dimensionless mean velocity in y direction	–
X	Dimensionless coordinate in x direction	–
Y	Dimensionless coordinate in y direction	–
Z	Dimensionless coordinate in z direction	–

Consent to participate The authors give consent to participate

Consent for publication The authors give consent for publication

Availability of data and materials Not applicable

Code availability Not applicable

Funding Open Access funding enabled and organized by Projekt DEAL.

Conflict of interest On behalf of all authors, the corresponding author states that there is no conflict of interest.

References

1. Baitinger G (2011) Multiskalenansatz mit Mikrostrukturanalyse zur Drallbeurteilung von Dichtungsgegenlaufflächen, Universität Stuttgart. PhD thesis, Dissertation
2. Bartarya G, Choudhury S (2016) Surface integrity issues in finish hard turning. In: Reference Module in Materials Science and Materials Engineering. https://doi.org/10.1016/B978-0-12-803581-8.04047-9
3. Baumann M (2017) Abdichtung drallbehafteter Dichtungsgegenlaufflächen-Messung, Analyse, Bewertung und Grenzen. PhD thesis, Universität Stuttgart
4. Börner R, Winkler S, Junge T et al (2018) Generation of functional surfaces by using a simulation tool for surface prediction and micro structuring of cold-working steel with ultrasonic vibration assisted face milling. J Mater Process Technol 255:749–759. https://doi.org/10.1016/j.jmatprotec.2018.01.027
5. Börner R, Penzel M, Junge T et al (2019) Design of deterministic microstructures as substrate pre-treatment for CVD diamond coating. Surfaces 2(3):497–519. https://doi.org/10.3390/surfaces2030037
6. Burkhart C, Thielen S, Sauer B (2020) Online determination of reverse pumping values of radial shaft seals and their tribologically equivalent system. Tribol Schmierungstech. https://doi.org/10.30419/TuS-2020-0025
7. Davim JP, Figueira L (2007) Comparative evaluation of conventional and wiper ceramic tools on cutting forces, surface roughness, and tool wear in hard turning AISI d2 steel. Proc Inst Mech Eng Part B J Eng Manuf 221(4):625–633. https://doi.org/10.1243/09544054jem762
8. DIN 3761-2 (1984) Din3761-2: Rotary shaft lip type seals for automobils; applications
9. Fehrenbacher C, Haas W (2015) 3D-Kennwerte: 3D-Oberflächenkennwerte für Dichtflächen: Abschlussbericht. Forschungsvorhaben Nr. 674 I.. Forschungsvereinigung Antriebstechnik eV (FVA)
10. Frölich D, Magyar B, Sauer B (2014) A comprehensive model of wear, friction and contact temperature in radial shaft seals. Wear 311(1–2):71–80. https://doi.org/10.1016/j.wear.2013.12.030
11. Gadari ME, Fatu A, Hajjam M (2016) Effect of grooved shaft on the rotary lip seal performance in transient condition: elasto-hydrodynamic simulations. Tribol Int 93:411–418. https://doi.org/10.1016/j.triboint.2015.09.031
12. Grzesik W (2008) Machining of hard materials. In: Machining. Springer, London, pp 97–126 https://doi.org/10.1007/978-1-84800-213-5_4
13. Grzesik W, Żak K, Kiszka P (2014) Comparison of surface textures generated in hard turning and grinding operations. Proc CIRP 13:84–89. https://doi.org/10.1016/j.procir.2014.04.015
14. Guo F, Jia X, Wang L et al (2016) The effect of axial position of contact zone on the performance of radial lip seals with a textur-

ing shaft surface. Tribol Int 97:499–508. https://doi.org/10.1016/j.triboint.2016.01.031
15. Guo Y, Yen DW (2004) Hard turning versus grinding—the effect of process-induced residual stress on rolling contact. Wear 256(3–4):393–399. https://doi.org/10.1016/s0043-1648(03)00443-5
16. Hamrock BJ, Schmid SR, Jacobson BO (2004) Fundamentals of fluid film lubrication. CRC Press https://doi.org/10.1201/9780203021187
17. Harp SR (2000) A computational method for evaluating cavitating flow between rough surfaces. PhD thesis, Georgia Institute of Technology
18. ISO 11562 (1996) ISO11562: Geometrical Product Specifications (GPS) – Surface texture: Profile method – Metrological characteristics of phase correct filters
19. Jia X, Jung S, Haas W et al (2012) Numerical simulation and experimental study of shaft pumping by plunge ground shafts with rotary lip seals. Tribol Int 48:155–161. https://doi.org/10.1016/j.triboint.2011.11.019
20. Kammüller M (1986) Zur Abdichtwirkung von Radial-Wellendichtringen. PhD thesis, Universitat Stuttgart
21. Kawahara Y, Hirabayashi H (1979) A study of sealing phenomena on oil seals. A S L E Trans 22(1):46–55. https://doi.org/10.1080/05698197908982901
22. Kligerman Y, Shinkarenko A (2011) The effect of tapered edges on lubrication regimes in surface-textured elastomer seals. Tribol Int 44(12):2059–2066. https://doi.org/10.1016/j.triboint.2011.09.004
23. Kunstfeld T (2005) Einfluss der Wellenoberfläche auf das Dichtverhalten von Radial-Wellendichtungen. PhD thesis, Universität Stuttgart
24. Lechner G, Raab H (1998) Influence of the shaft running surface on the sealing behaviour of radial shaft seals: research project. Final report, BMWi/AiF, (10670), pp 59–73
25. Martell JJ, Liu CR, Shi J (2014) Experimental investigation on variation of machined residual stresses by turning and grinding of hardened AISI 1053 steel. Int J Adv Manuf Technol 74(9–12):1381–1392. https://doi.org/10.1007/s00170-014-6089-8
26. Matus TM, Leichner (2017) Auswirkung stochastischer Strukturen von Gegenlaufflächen auf dieFunktion von Radialwellendichtringen. FVA 706. Forschungsvereinigung Antriebstechnik eV (Forschungsbericht)
27. Mazumder S (2015) Numerical methods for partial differential equations: finite difference and finite volume methods. Academic Press
28. MBN 31007-7:2009-04 (2009) MBN 31007-7:2009-04. Geometrische Produktspezifikationen (GPS) -Oberflächenbeschaffenheit. Mess- und Auswerteverfahren zur Bewertung von drallreduzierten dynamischen Dichtflächen
29. Patir N, Cheng HS (1978) An average flow model for determining effects of three-dimensional roughness on partial hydrodynamic lubrication. J Lubr Technol 100(1):12–17. https://doi.org/10.1115/1.3453103
30. Patir N, Cheng HS (1979) Application of average flow model to lubrication between rough sliding surfaces. J Lubr Technol 101(2):220–229. https://doi.org/10.1115/1.3453329
31. Raid I, Seewig J, Frölich D et al (2014) Kinematische Simulation gedrehter Wellenlaufflächen. Wt Werkstatttech Online 104:279–287
32. Remppis M (2016) Untersuchungen zum Förderverhalten von Dichtsystemen mit Radial-Wellendichtringen aus Elastomer. PhD thesis, Universität Stuttgart
33. Rocke AH, Salant RF (2005) Elastohydrodynamic analysis of a rotary lip seal using flow factors. Tribol Trans 48(3):308–316. https://doi.org/10.1080/05698190590965639
34. Salant RF (1999) Theory of lubrication of elastomeric rotary shaft seals. Proc Inst Mech Eng Part J J Eng Tribol 213(3):189–201. https://doi.org/10.1243/1350650991542938
35. Salant RF (2010) Soft elastohydrodynamic analysis of rotary lip seals. Proc Inst Mech Eng Part C J Mech Eng Sci 224(12):2637–2647. https://doi.org/10.1243/09544062jmes2181
36. Seewig J, Hercke T (2009) Lead characterisation by an objective evaluation method. Wear 266(5–6):530–533. https://doi.org/10.1016/j.wear.2008.04.080
37. Sonnemann R (2006) Abdichten von hartgedrehten Hinterachseingangswellen. Z Prax Dichtungstech 9
38. Thielen S, Magyar B, Sauer B et al (2018) Functional investigation of zero lead radial shaft seal counter-surfaces turned with a special method. Tribol Int 118:442–450. https://doi.org/10.1016/j.triboint.2017.02.002
39. Thielen S, Magyar B, Sauer B (2020) Thermoelastohydrodynamic lubrication simulation of radial shaft sealing rings. J Tribol. https://doi.org/10.1115/1.4045802
40. Thielen S, Breuninger P, Hotz H et al (2021) Improving the tribological properties of radial shaft seal countersurfaces using experimental micro peening and classical shot peening processes. Tribol Int 155:106764. https://doi.org/10.1016/j.triboint.2020.106764
41. Vogt R (1997) Alternative Bearbeitungsmethoden von Wellenoberflächen Tribologische Partner. Kem Konstr Elektronik Maschinenbau 5:45
42. Woloszynski T, Podsiadlo P, Stachowiak GW (2015) Efficient solution to the cavitation problem in hydrodynamic lubrication. Tribol Lett. https://doi.org/10.1007/s11249-015-0487-4